

High-impact resistant hollow glass microsphere-filled polypropylene/polyamide 6 blends via reactive compatibilization

Monica Tanniru and Pankaj Tambe*

School of Mechanical Engineering, VIT-AP University, Amravati – 522237, Andhra Pradesh, India.

Received: 22 March 2023, Accepted: 29 April 2023

ABSTRACT

The automotive industry has a significant need for composites made of high impact strength polymer blends. Melt-mixing was used in this work to reinforce hollow glass microspheres (HGMs) with 50:50 polypropylene/polyamide 6 (PP/PA6) blends. Using FTIR spectroscopy, it is observed that the 50PP50PA6 blend is compatibilized with maleated PP, producing a reactively compatible blend. The compatibilization process has refined the morphology of the 50PP50PA6 blend. Additionally, the incorporation of HGMs into the 50PP50PA6 blend produced a finer blend morphology, which helped to enhance the crystallinity of the polymer phase and mechanical properties to the maximum. The tensile modulus and impact strength of a 50PP50PA6 blend with maleated PP that contains 3 wt.% HGMs are better than those of a neat blend by 15.6% and 90.1%, respectively. Fractography was used to identify the fracture mechanism which reveals the retention of droplets over the surface of impact specimens of HGMs-filled compatibilized PP/PA6 blend. When 50PP50PA6 blend with and without maleated PP is filled with HGMs, rheological characterization shows that the blend viscosity has decreased, indicating improved processability. Dynamic mechanical analysis (DMA) revealed that the incorporation of HGMs into the 50PP50PA6 blend enhances the storage modulus. **Polyolefins J (2023) 10: 177-190**

Keywords: Polypropylene (PP); polyamide 6 (PA6); blends; hollow glass microsphere (HGMs); composites.

INTRODUCTION

Polypropylene (PP) is a thermoplastic commodity polymer that is extensively used in industry for a variety of purposes [1-3]. It is used because of its ease of processing, low melting point, and high tensile strength [3]. However, PP has a disadvantage in terms of impact properties [4]. To overcome this disadvantage, many researchers have attempted to create PP blend systems

with various rubbery polymers [5]. Several studies have been published on the PP/ABS based blend, where the ABS can improve the impact properties of the PP [5-7]. Another polymer that can be blended with PP to improve mechanical properties is polyamide 6 (PA6) [8-10]. PA6 is an engineering plastic that has been widely used because

*Corresponding Authors - E-mail: pbtambe2010@gmail.com

of its high impact strength and durability. Shi et al. [9] utilized PP grafted maleic anhydride (PP-g-MA) to develop emulsion morphology for a compatible PP/PA6 blend. Palacios et al. [11] discovered that an 80/20 (wt/wt) PP/PA6 blend compatibilized with maleated PP reveals the development of matrix-droplet morphology. Pinheiro et al. [12] attempted in-situ monitoring of the PA6 blends compatibility with PP-g-MA and PP grafted acrylic acid (PP-g-AA). Due to compatibility, a copolymer of PP and PA6 is formed in the interphase [11]. According to the literature, maleated polypropylene is a commonly used compatibilizer in compatible PP/PA6 blends [9-12]. The compatibilized PP/PA6 blends using maleated PP can refine the morphology and results in improved mechanical properties. As a result, the PP-g-MA is utilized as a compatibilizer to make PP/PA6 blends compatible in this work.

Hollow glass microspheres (HGMs) are a popular filler material for thermoplastic-based composites [13-16]. HGMs are spherical hollow particles with a hard space and an inert gas at their core. The main benefit of HGMs is their low density and high thermal conductivity. HGMs-filled PP composites were processed by Gogoi et al. [17] for thermal management applications in the automobile industry. Along with PP-g-MA, they added 5 to 40 wt.% HGMs and 5-8 wt.% carbon fiber to the PP matrix. The incorporation of 20 wt.% HGMs and 5 wt.% carbon fibre in the PP matrix can enhance the thermal stability. Kang et al. [18] improved flame retardancy by incorporating HGMs and intumescent flame retardants (IFR) into the PP matrix. The cone calorimetry results showed that HGMs- and IFR-filled PP composites have a 55% reduction in peak heat release rate (HRR). Yagci et al. [19] demonstrated that adding 1-15 wt.% HGMs to PP composite improves thermal stability and stiffness. A

review of the literature on HGMs-filled PP composites reveals an improvement in properties. Furthermore, HGMs-filled PP composites are commercially available for weight reduction in the automobile industry. Aside from weight-saving materials, the mechanical properties of materials must be improved in order to reduce weight with design changes. Thus, HGMs are used as filler material in this work due to their low cost and potential weight savings.

From the discussion so far, it is clear that the maleated PP has to be added for the enhancement in mechanical properties of PP-based blends. HGMs being a hollow nature can improve the impact properties of the PP-based blends. With the above aspect into consideration, in this study, HGMs were mixed with a PP/PA6 blend in the presence of compatibilizer to better understand the morphology, crystallinity, and mechanical property relationship. The PP/PA6 ratio is 50:50, which is referred to as the 50PP50PA6 blend. In the 50PP50PA6 blend, the compatibilizer PP-g-MA was added at a rate of 5% by weight. Several characterization techniques were used to characterize 50PP50PA6 blends and their composites.

EXPERIMENTAL

Experimental setup

Table 1 shows the materials used in this work in detail.

Blend Composites Processing

The blend composition of the specimens with codes is shown in Table 2. As per the compositions, the processing was done by melt-mixing. The melt-extrusion of HGMs-mixed 50PP50PA6 blend and their composites with and without PP-g-MA was performed using an Asabi Machinery twin-screw extruder from India. It is a co-rotating extruder with

Table 1. Details of raw materials used in the work.

Name of Raw Materials	Company	Remarks
Polypropylene (PP)	Reliance Industries, India	REPOL 110MA; Melt flow index of 11 g/10 min @ 230°C with a load of 2.16 kg
Polyamide-6 (PA6)	GSFC, Gujrat, India	Melt flow index of MFI of 25 g/10 min @ 260°C with a load of 2.16 kg
Polypropylene grafted maleic anhydride (PP-g-MA)	Pluss Polymer Ltd, India	Melt flow index of 14 g/10 min @ 230°C with a load of 2.16 kg
Hollow glass microspheres (HGMs)	3 M India, India	Dispersion grade
Tetrahydrofurane	S.D. Fine Chemicals, India.	AR grade

a length-to-diameter (L/D) ratio of 32 and a D of 25 mm, operating at temperatures ranging from 205-225-245°C and a screw speed of 60 rpm. The strand of blend composites has been palletized. The chopped granules were then injection moulded at 250-265-275°C, 80 rpm rotational speed, and 7 bar pressure. Disha Impex, India, manufactured injection moulding machine was used. The materials were vacuum dried at 85°C before each processing step to remove moisture.

Characterization

HGMs characterizations were done through Fourier transform infrared (FTIR) spectroscopy of Bruker, Germany. It was done in the scanning range of 400-4000 cm^{-1} . Further, FTIR of 50PP50PA6 blends and their composites was done in the same scanning range. The scanning electron microscopy (SEM) of Carl Zeiss, Germany, was used to taking the images of HGMs. In addition, SEM images of cryo-fractured 50PP50PA6 blends and their composites specimens were taken to study the morphology development. Additionally, SEM images of tensile and impact failure specimens were taken to study the fracture behaviour. Wide-angle X-ray diffractometry (WAXRD) was performed over 50PP50PA6 blends and their composites on D8 Advance, BRUKER. It was done with a wavelength of 1.54 nm and a scanning range of 10–90°. Rheology of 50PP50PA6 blends and their composites was done through the rheometer of Anton Parr. The steady-state shear mode characterization was done with Peltier plate heating at 230°C in the shear rate range as 0.001-20 1/s at cone and plate arrangement. The diameter of cone is 25 mm. Dynamic mechanical analysis (DMA) was done on 50PP50PA6 blends and their composites through PerkinElmer in flexural arrangement. The temperature range of -40 to 170°C at 1Hz under a heating rate of 3°C/min was maintained. Tensile testing of 50PP50PA6 blends and their composites

Table 2. Codes of HGMs-filled 50/50 (wt%/wt.%) PP/PA6 blends and their composites in the presence and absence of compatibilizer.

Sample codes	PP (wt%)	PA6 (wt%)	HGMs (wt%)	PP-g-MA (wt%)
50PP50PA	50	50	0	0
50PP50PA5C	47.5	47.5	0	5
50PP50PA3HGM	48.5	19.5	3	0
50PP50PA5C3HGM	46	46	3	5

was done over UTM of Tinius Olsen, UK (H10KL). The ASTM D638 protocol was used for tensile testing. The impact testing was done in over a pendulum impact tester. The testing was performed as per ASTM D256 on International Instruments, India made over 50PP50PA6 blends and their composites un-notched specimens. Differential scanning calorimetry (DSC) of 50PP50PA6 blends and their composites was done over NETZSCH DSC 204 F1 PHOENIX. It has been done in heating-cooling-heating mode with conditions as 30 to 265°C under a heating rate of 10°/min. The percent crystallinity (X_c) was calculated as $X_c = (\Delta H_{\text{norm}}) / (\Delta H_{100})$. Where (ΔH_{norm}) is the normalized heat of fusion (ΔH_{norm}) and (ΔH_{100}) is the heat of fusion of 100% crystalline PP or PA6 phase. The (ΔH_{100}) values are as follows: PP = 207 J/g and PA6 = 204.8 J/g, respectively [20, 21].

RESULTS AND DISCUSSION

Characterization of HGMs

The SEM was used to characterize the HGMs. Figure 1 shows a SEM image of the HGMs. The SEM image reveals HGMs with varying sizes ranging from 10 to 50 μm . The SEM image shows that the surface of the HGMs is rough. The FTIR spectra of the HGMs powder received were recorded. Figure 2 depicts the FTIR spectra of HGMs powder. Since the HGMs used are made of borosilicate glass, there are two peaks at wavenumbers of 796 cm^{-1} and 1056 cm^{-1} . These two peaks appeared correspond to the asymmetric stretching of Si-O of HGMs [22]. Furthermore, an O-Si-O bond is present at 497 cm^{-1} due to symmetric stretching [23-24]. Because of moisture absorption, the peak at 497 cm^{-1} is of the -OH group.

Morphology, Interface and Rheological Studies of HGMs-filled Blend Composites

The interaction between the solid reinforcement and the polymer determines morphology development [11]. Furthermore, the interaction of two polymers in the presence of a compatibilizer determines the development of morphology [12]. Initially, an interfacial calculation was performed among PP, PA6, and HGMs to determine the filler-polymer affinity. Wu's [25] interfacial calculation can be written as

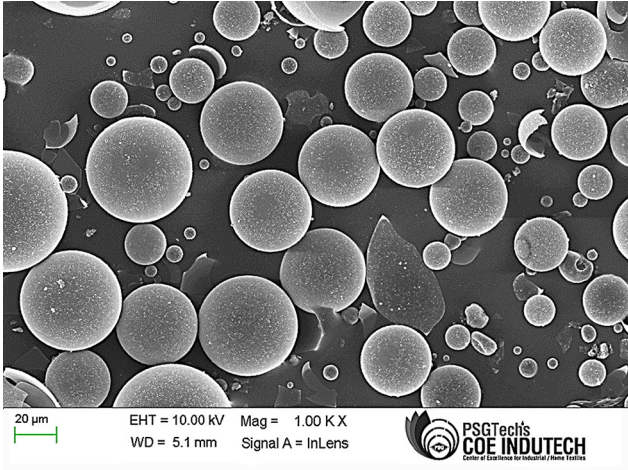


Figure 1. SEM image of HGMs.

follows.

$$\gamma_{fp} = \gamma_p + \gamma_f - 2\left(\sqrt{\gamma_f^D \gamma_p^D} + \sqrt{\gamma_f^P \gamma_p^P}\right) \quad (1)$$

Where, γ_{fp} is the surface energy (SE) between filler (*f*) and polymer (*p*), γ_s is the SE of filler, γ_p is the SE of the polymer melt, γ_s^D and γ_l^D are the dispersive parts of the SE of *f* and *p*, γ_s^P and γ_l^P are the polar part of the SE of *f* and *p*. From literature, the surface energies of polymers and HGMs are noted and tabulated in Table 3 [26-28]. With equation 1, the γ_{fp} calculated for pair of PP-HGMs is 27.2 mJ/m². While the γ_{fp} calculated for pair of PA6-HGMs is 5.3 mJ/m². The surface energy pair value of PA6-HGMs is lower in comparison with that of PP-HGMs pair, indicating a preferential interaction between the PA6 and HGMs. FTIR spectroscopy was performed on the 50PP50PA6 blend and their composite specimens to determine the interaction between the PA6 and HGMs. In addition,

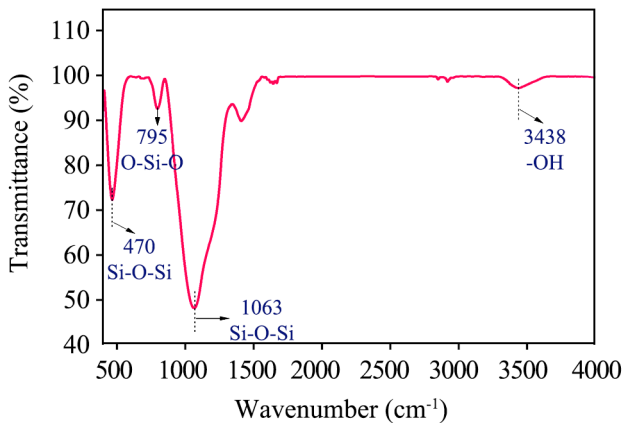


Figure 2. FTIR spectra of HGMs.

Table 3. Surface free energies (γ_s) and their dispersive (γ_s^D) and polar (γ_s^P) components of the materials used.

Sample	Surface free energy (mJ/m ²)			References
	γ_s	γ_s^P	γ_s^D	
PA6	29.8	6.4	23.4	26
PP	22	0.4	21.6	27
HGMs	74.0	34.2	39.8	28

the melt interfacial reaction between the PP-g-MA and PA6 should be established. The FTIR spectra of blend composites are shown in Figure 3. Figure 3a shows the FTIR of 50PP50PA6 blend and 50PP50PA6 blend containing PP-g-MA. It was known that the maleic anhydride group of PP-g-MA happens to react with the amine group of PA6 and forms an imide linkage [29]. The cyclic imide peak appeared at 715 cm⁻¹ in case of 50PP50PA6 blend containing PP-g-MA, while the absence of this peak in 50PP50PA6 blend depict the melt interfacial reaction between PP-g-MA

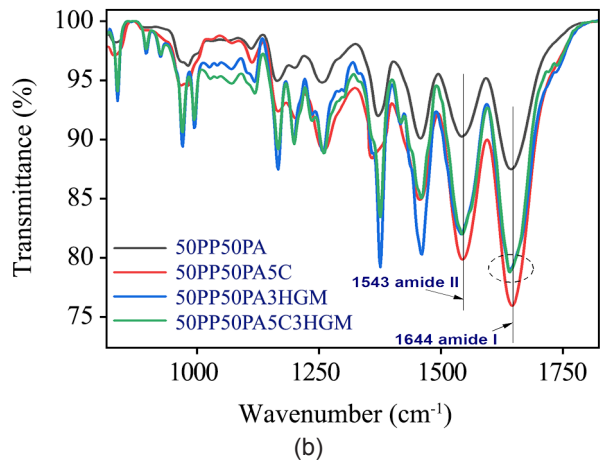
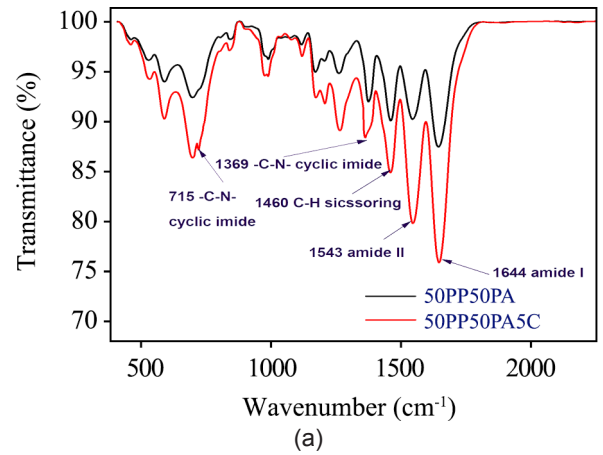


Figure 3. FTIR spectrum of 50/50 PP/PA6 blends with 3wt% HGMs in the presence and absence of PP-g-MA.

and PA6. Figure 3b shows the FTIR of 50PP50PA6 blends and their composites containing PP-g-MA. The peak at 1644 cm^{-1} is caused by amide I and is associated with the N-H bending of the PA6 phase. While the 1543 cm^{-1} peak is caused by amide II and is associated with the C-N bending of the PA6 phase [29]. These peaks of amide I and amide II can be seen in a specimen of 50PP50PA6 blend containing PP-g-MA. However, the FTIR spectra of HGMs-filled 50PP50PA6 blend containing PP-g-MA show a peak shift of amide I, which is circled in Figure 3, indicating an interaction between the HGMs and the PA6 phase. During extrusion, a melt-interfacial reaction occurs with imide bond formation for PA6/PP blend with the addition of PP-g-MA [29]. The -C-N peak of cyclic imide bond appears at 1543 cm^{-1} , which has the same wavenumber as amide II of PA6 [30].

Rheological characterization can be used to further investigate the dispersion and interaction of HGMs with polymers. Furthermore, the influence of melt interfacial reaction can be investigated using rheological characterization. The viscosity vs. shear rate of 50PP50PA6 and their composites are represented in Figure 4. All 50PP50PA6 compositions and composites exhibit decreased viscosity values corresponding to increased shear rate, confirming the shear thinning behaviour. Table 4 shows the viscosity of the 50PP50PA6 blends and their composites with a constant shear rate of 10 s^{-1} . The 50PP50PA6 blend has a viscosity of $1.5 \times 10^4\text{ mPa}\cdot\text{s}$, while the 50PP50PA6 blend containing PP-g-MA shows a viscosity of $7.9 \times$

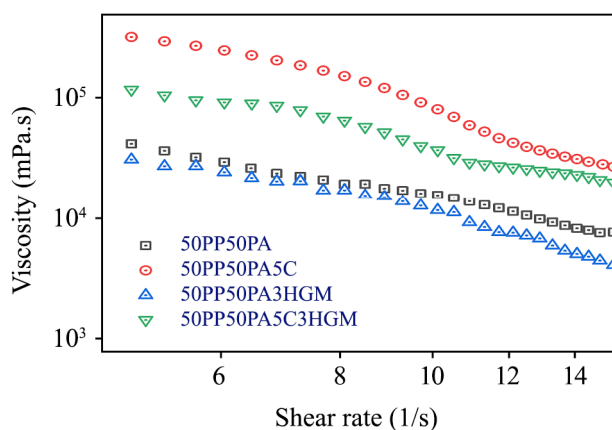


Figure 4. Steady shear rheology of pure blend and HGMs-filled 50PP50PA6 blends and their composites in the presence and absence of PP-g-MA.

Table 4. Viscosity and power law index of 50/50 (wt/wt) PP/PA6 blends in the presence and absence of HGMs and PP-g-MA.

Sample code	Viscosity at 10 (1/s)	n
50PP50PA	1.5×10^4	0.29
50PP50PA5C	7.9×10^4	0.89
50PP50PA3HGM	1.3×10^4	0.32
50PP50PA53HGM	3.6×10^5	0.51

$10^5\text{ mPa}\cdot\text{s}$. This observation reveals that the viscosity of 50PP50PA6 blend compatibilized with PP-g-MA increases as compared to that of 50PP50PA6 blend. Whereas the incorporation of 3 wt.% HGM in a 50PP50PA6 blend shows a viscosity of $1.3 \times 10^4\text{ mPa}\cdot\text{s}$. Furthermore, the incorporation of 3 wt.% HGM in 50PP50PA6 blend with PP-g-MA is $3.6 \times 10^5\text{ mPa}\cdot\text{s}$. It may be associated with the melt-interfacial reaction between PP-g-MA and PA6. In comparison to neat blend composition, the incorporation of HGMs in 50PP50PA6 and 50PP50PA6 containing PP-g-MA results in lower viscosity. To comprehend the observed viscous behaviour of 50PP50PA6 blends and their composites, it is necessary to know the evolution of morphology. Figure 5 depicts the morphology development of 50PP50PA6 blends and their composites. The cryo-fractured and etched SEM image of 50PP50PA6 (Figure 5a) shows the development of co-continuous morphology containing droplets. Because the PA6 phase was etched from all of the 50PP50PA6 blends and their composites, the droplets observed in Figure 5a are of the PA6 phase. This finding confirms the development of complex morphology in the 50PP50PA6 blend (Figure 5a). The incorporation of the compatibilizer PP-g-MA in 50PP50PA6 blend results in the formation of refined co-continuous morphology with reduced ligament thickness and droplets (Figure 5b). When HGMs are added to a 50PP50PA6 blend, the elongated fibrils in the matrix with PA6 etched out appear as holes (Figure 5c). The fibril is caused by shear thinning behaviors and pressure variation in the mould cavity caused by the injection moulding process. Elongated fibril formation was previously observed in the PA6/PP blend [31]. With an incorporation of HGMs and PP-g-MA in 50PP50PA6 blend, the density of PA6 droplets increases (Figure 5d). It should be noted that reactive compatibilization limited droplet migration from the PP phase, which is responsible for finer

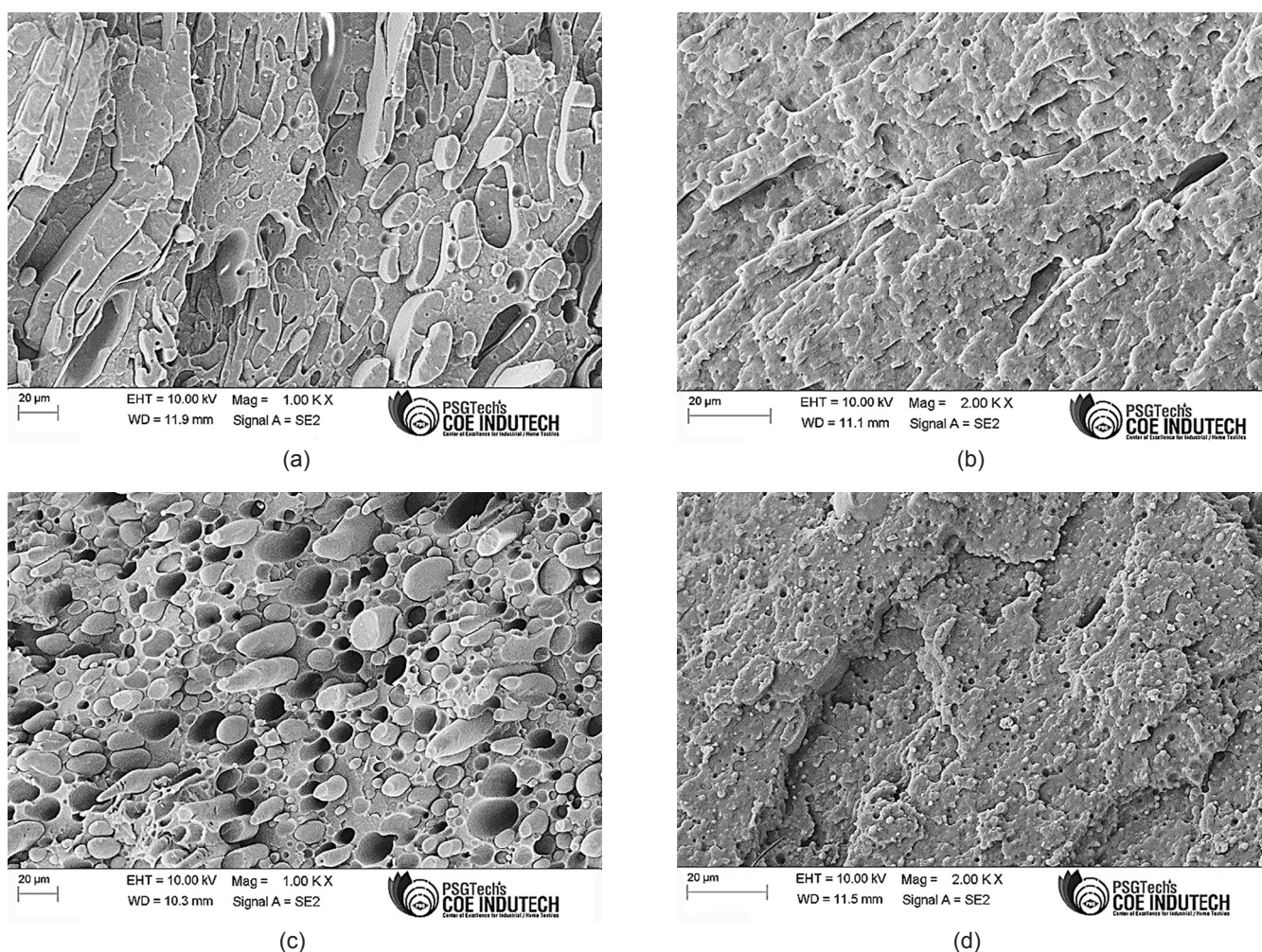


Figure 5. SEM images of cryo-fractured (a) 50PP50PA (b) 50PP50PA5C (c) 50PP50PA3HGM (d) 50PP50PA5C3HGM.

droplet retention.

The morphology development of the blend can be correlated with the rheology. The power law equation is recommended for fitting the shear thinning behavior which is $\eta(\dot{\gamma}) = K\dot{\gamma}^{n-1}$. Where $\eta(\dot{\gamma})$ is the viscosity of the blend at varying shear rates ($\dot{\gamma}$), K is consistency, and n is the power law index. Table 4 shows the estimated values of n obtained by fitting the power law equation. The 50PP50PA6 blend has a value of 0.29, which is significantly lower because there is no interaction between the PP and PA6 phases. But, the n value for 50PP50PA6 blend containing the compatibilizer PP-g-MA is 0.89. This clearly shows that the n value of 50PP50PA6 blend containing compatibilizer PP-g-MA is significantly increased because of the reaction between PP-g-MA and PA6 phase (FTIR spectroscopy in Figure 2). Further, the refined morphology of the 50PP50PA6 blend containing compatibilizer PP-g-MA shows high viscosity value, confirming higher

Newtonian nature. The incorporation of 3 wt.% HGMs to the 50PP50PA6 blend raises the n value to 0.32 from 0.29 for the 50PP50PA6 blend. It is because of the development of morphology in the form of fibrils for HGMs-filled 50PP50PA6 blend. The viscosity is slightly lower for HGM-filled 50PP50PA6 blend because of the bending of the fibrils in the shear direction. As a result, the presence of HGMs in the 50PP50PA6 blend influences the morphology and flow behaviour. In addition, incorporating 3 wt.% HGM in 50PP50PA6 blends containing compatibilizer PP-g-MA yields n value of 0.51. This n value is greater than that of the 50PP50PA6 blend with HGMs. The compatibilization action of the 50PP50PA6 blend with HGMs and PP-g-MA increases the viscosity. However, in comparison with the neat 50PP50PA6 blend with PP-g-MA, the viscosity of the 50PP50PA6 blend containing PP-g-MA and HGMs is lower, indicating that the HGMs improves the processability

of the 50PP50PA6 blend. The reason is that the finer droplets of PA6 were retained in the PP phase, which helps to improve the processability of 50PP50PA6 blends with PP-*g*-MA and HGMs.

WAXRD and Crystallization Studies of HGMs-filled Blend Composites

The WAXRD was performed on the 50PP50PA6 blends and their composites to better understand the crystal structure formation during the processing of PP/PA6 blends and their composites. Figure 6 depicts the WAXRD of 50PP50PA6 blends and composites. It demonstrates the peak at 2θ of 14.1° , which is the (110) plane of α -form PP crystals for the 50PP50PA6 blend. For the 50PP50PA6 blend, there are two additional peaks at 2θ of 16.9° and 18.6° for the (040) plane and (130) plane related to α -form PP crystals [20, 21]. Figure 6 also shows two peaks at 2θ of 20.1° and 23.3° , which correspond to the (200) and (002) planes of the α -form of PA6 crystals for the 50PP50PA6 blend [29]. For the 50PP50PA6 blend, there is a peak at 2θ of 21.3° that is reflected in the PP and PA6 phases. All of the peaks listed above were found in the 50PP50PA6 blend with PP-*g*-MA. The incorporation of HGMs in the 50PP50PA6 blend results in the appearance of a sharp peak at 21.3° , while the other peaks related to PA6 crystals at 20.1° and 23.3° do not appear. The large amount of PP at the sample's surface is made possible by the decrease in viscosity of the 50PP50PA6 blend, since WAXRD was done over the injection moulded specimens. That is why the α -form of PA6 did not

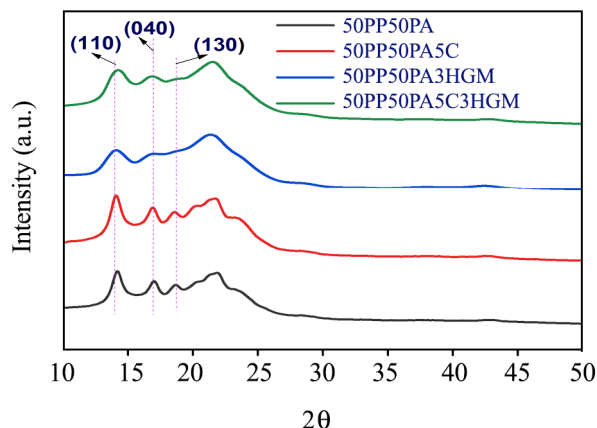


Figure 6. WAXD of pure blend and HGMs-filled 50/50 PP/PA6 blends and their composites in the presence and absence of PP-*g*-MA.

appear prominently in the WAXRD peaks (PA6 crystals at 20.1° and 23.3°). A similar observation was made when HGMs were included in the 50PP50PA6 blend containing PP-*g*-MA.

The crystallization behaviour of 50PP50PA6 blends and their composites was studied using DSC. The crystallization exotherms and melting endotherms of the 50PP50PA6 blends and their composites are shown in Figure 7. Figure 7a depicts the crystallization exotherms for the PA6 phase at temperatures ranging from 170 - 195°C . While the PP phase exhibits crystallization exotherms in the temperature range of 105 - 135°C . For the 50PP50PA6 blend, the crystallization temperature (T_c) of PP is 118.9°C and the T_c of PA6 is 187.4°C . The incorporation of the compatibilizer PP-*g*-MA in 50PP50PA6 blend raises

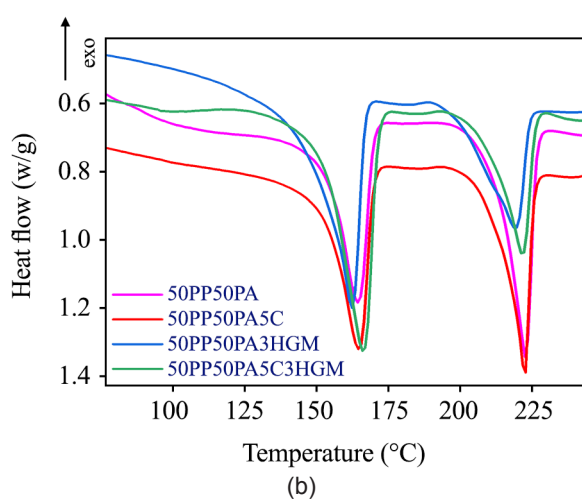
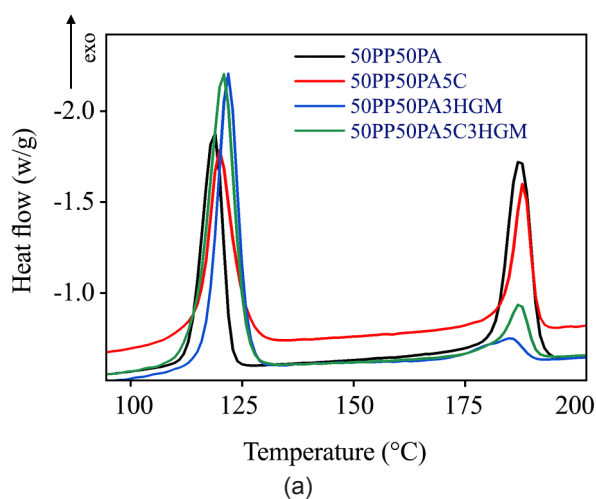


Figure 7. DSC (a) crystallization exotherms and (b) melting endotherms of pure blend and HGMs-filled 50/50 PP/PA6 blends and their composites in the presence and absence of PP-*g*-MA.

the T_c of the PP and PA phases, which is associated with refinement in morphology development and the reaction between PP-g-MA and PA6. The refined morphology will have a large surface area of contact, which causes the crystallization temperature to rise. The T_c of a PP phase for 50PP50PA6 blend containing 3 wt.% HGMs shows a significant improvement. It is the development of the fibrillar morphology of the PA6 phase responsible for the increase in T_c for 50PP50PA6 blend containing 3 wt.% HGMs. The another reason of refinement morphology is the increased surface area of contact between the crystallized PA6 phase and PP phase for 50PP50PA6 blend containing 3 wt.% HGMs. Furthermore, combining HGMs and PP-g-MA with 50PP50PA6 blend reveals a lower enhancement in the T_c of the PP phase when compared to HGMs-filled 50PP50PA6 blends containing PP-g-MA. The increase is associated with further refinement in morphology for HGMs- and PP-g-MA-filled 50PP50PA6 blend in comparison with the neat blend. In addition, the interaction between the PA6 phase and HGMs lowers the T_c of the PA6 phase.

Figure 7b depicts the melting endotherm of the 50PP50PA6 blend and its composite. Figure 7b depicts the two melting endotherms for the PA6 and PP phases, which are centered at 185-230°C and 130-175°C, respectively. The crystallinity of the polymer phases was calculated using the area under the melting endotherms. The melting temperature (T_m) of 50PP50PA6 blend containing PP-g-MA shows a shift as compared to 50PP50PA6 blend, depicting the reactive compatibilization of the blend. The percentage crystallinity of the PP and PA6 phases of the 50PP50PA6 blend is 36.4% and 38.8%, respectively. The incorporation of compatibilizer PP-g-MA in the 50PP50PA6 blend results in a 41.2% increase in the crystallinity of the PA6 phase in comparison with the neat blend, whereas the PP phase remains unaffected. It may be due to morphological refinement, and there is an interfacial reaction between PA6 and the PP phase. By incorporating 3% by weight of HGM in the 50PP50PA6 blend, the crystallinity of PA6 increased to 43.8% compared to the neat blend. While the crystallinity of the PP phase increased to 57.1% in comparison with the neat blend. The formation of fibrillar morphology is responsible for the significant enhancement in the

crystallinity of the PP phase. The PA6 phase must crystallize first, followed by the PP phase. Since the PA6 phase crystallizes early, it can act as a heterogeneous nucleating site, thus the crystallinity of PP increases. The interaction of HGMs with PA6 phase for 3wt% of the HGMs in 50PP50PA6 blend causes an increase in the PA6 phase crystallinity. The incorporation of 3 wt.% HGMs in the 50PP50PA6 blend containing PP-g-MA increases the percentage crystallinity of the PA6 phase to 52.3%, and the percentage crystallinity of the PP phase to 62.5% in comparison with the neat blend. This is due to the refinement of morphology seen in Figure 5d, which contributes to the crystallinity of the PA6 and PP phases.

DMA Studies of HGMs-filled Blend Composites

DMA tests were performed on the HGMs-filled 50PP50PA6 blend and its composites. The storage modulus (E') and loss tangent ($\tan\delta$) of the HGMs-filled 50PP50PA6 blends and their composites are shown in Figure 8. The E' vs. temperature of the HGMs-filled 50PP50PA6 blends and their composites are shown in Figure 8a. At -35°C, the E' value of 50PP50PA6 blend is 2910 MPa. The compatibility of the 50PP50PA6 blend with PP-g-MA reveals an E' value of 3343 MPa at -35°C. The increase in the E' value due to the compatibilization of the 50PP50PA6 blend with PP-g-MA represents the energy storage capacity. Further, the addition of 3% HGMs to 50PP50PA6 blends and their composites resulted in an E' value of 3343 MPa at -35°C. This observation indicates that the presence of HGMs in the 50PP50PA6 blend stiffens the surface in contact with the 50PP50PA6 blend. The incorporation of 3% HGMs in 50PP50PA6 and its composites containing PP-g-MA resulted in an E' value of 4302 MPa at -35°C. It indicates that the presence of roughly surfaced HGMs and the interfacial reaction between the PP and PA6 using the compatibilizer PP-g-MA cause the highest enhancement in the E' value.

The $\tan\delta$ vs. temperature of the HGMs-filled 50PP50PA6 blends and their composites is shown in Figure 8b. It depicts the two peaks at 5°C and 54°C associated with the 50PP50PA6 blend's glass transition (T_g) peak. The peak at 5°C represents the T_g of β -relaxation of the PP phase. Furthermore, the peak at 54°C is the T_g associated with the PA6 phase's

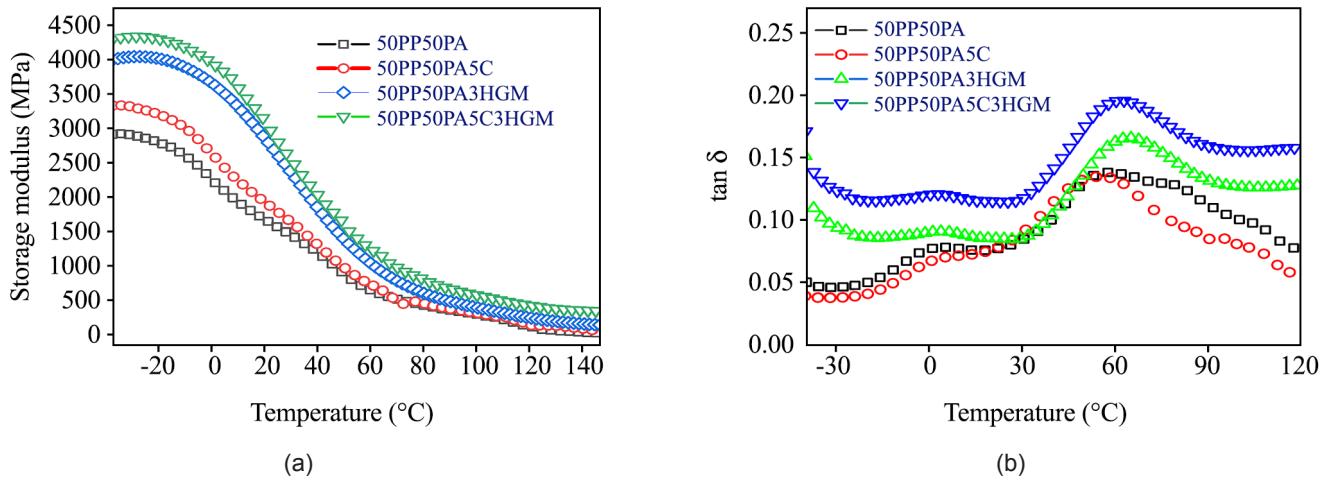


Figure 8. DMA curves: Temperature dependent (a) Storage Modulus and (b) Tan Delta of pure blend and HGMs-filled 50/50 PP/PA6 blends and their composites in the presence and absence of PP-g-MA.

α -relaxation. The 50PP50PA6 blend and its composites show no shift in the T_g peak of PP (β -relaxation). The presence of HGMs in the 50PP50PA6 blend and its composites causes a peak shift in the T_g peak of PA6 (α -relaxation). A significant peak shift at 54°C for HGMs-filled 50PP50PA6 blends and their composites is possible due to HGMs localization in the PA6 phase; additionally, the interaction between the PA6 phase and HGMs was established previously using FTIR spectroscopy.

Tensile and Impact Studies of HGMs-filled Blend Composites

Mechanical testing was done over 50PP50PA6 blends and composites to determine the correlation among morphology, crystallinity, and mechanical properties. The results of a tensile test performed

on the 50PP50PA6 blends and their composites are shown in Figure 9. Figure 9a displays the tensile modulus of 50PP50PA6 blends and their composites. The tensile modulus for the 50PP50PA6 blend is 610 MPa. The tensile modulus of the 50PP50PA6 blend increased by 5.4% to 643 MPa in comparison with the neat blend when the compatibilizer PP-g-MA was added. The tensile modulus of the 50PP50PA6 blend increased by 8.3% to 661 MPa when 3% HGMs were added as compared to the neat blend. In addition, the tensile modulus of 50PP50PA6 blends containing HGMs and PP-g-MA increased by 15.6% to 705 MPa as compared to the neat blend. Figure 9b displays the tensile strength of 50PP50PA6 blends and their composites. The tensile strength of the 50PP50PA6 blend is 16.5 MPa. The PP-g-MA-containing 50PP50PA6 blend's tensile strength increased to 26.8

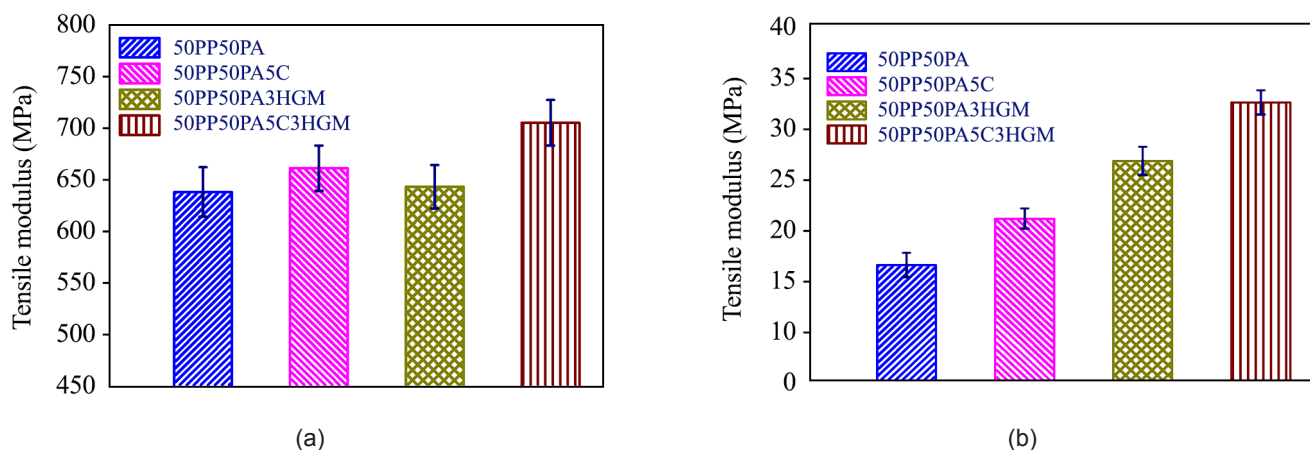


Figure 9. (a) Tensile Modulus and (b) Tensile Strength of 50/50 PP/PA6 blends and their composites in the presence and absence of PP-g-MA and HGMs.

MPa, which is 62.7% increase in comparison with the control blend. While the 50PP50PA6 blend's tensile strength increased by 27.8% to 21.1 MPa with the addition of 3% HGMs as compared to the neat blend. Furthermore, the tensile strength of 50PP50PA6 blend impressively increased by 97.5% to 32.6 MPa due to the addition of HGMs and PP-g-MA as compared to that of neat blend. The tensile behavior observed for 50PP50PA6 blends and their composites can be explained based on the morphology development and crystallization behavior.

The SEM of 50PP50PA6 blends and their composites is represented in Figure 10. The tensile fracture specimen of the 50PP50PA6 blend shows fibril formation (Figure 10a). The formation of fibrils is caused by the tensile elongation of amorphous chains and the unfolding of crystalline lamellae of the PP as well as PA6 phases. Tensile fracture of 50PP50PA6 blend with PP-g-MA compatibilizer reveals the formation of finer fibrils (Figure 10b).

Finer fibrils are formed by refining the morphology of the 50PP50PA6 blend containing PP-g-MA. Figure 10c reveals the formation of finer fibrils in the 3 wt.% HGMs-filled 50PP50PA6 blend when compared to the 50PP50PA6 blend. Figure 10d represents refined fibril formation after the incorporation of 3 wt.% HGMs in the 50PP50PA6 blend containing PP-g-MA. The SEM image in Figure 10d shows the presence of HGMs, which do not break, and the polymer chain of PP/PA6 slips past the HGMs due to non-covalent interaction.

The crystallinity, morphology, and fractured SEM images can explain the enhancement in tensile properties. The refinement in morphology (Figure 5), the melt-interfacial reaction between the PP-g-MA and PA6 phases (Figure 3), finer fibril formation (Figure 10), and increased crystallinity of a PA6 phase contribute towards enhancement in tensile properties of the 50PP50PA6 blend containing PP-g-MA. Further, the incorporation of HGMs in the 50PP50PA6 blend results in the formation of fibrils (Figure 10),

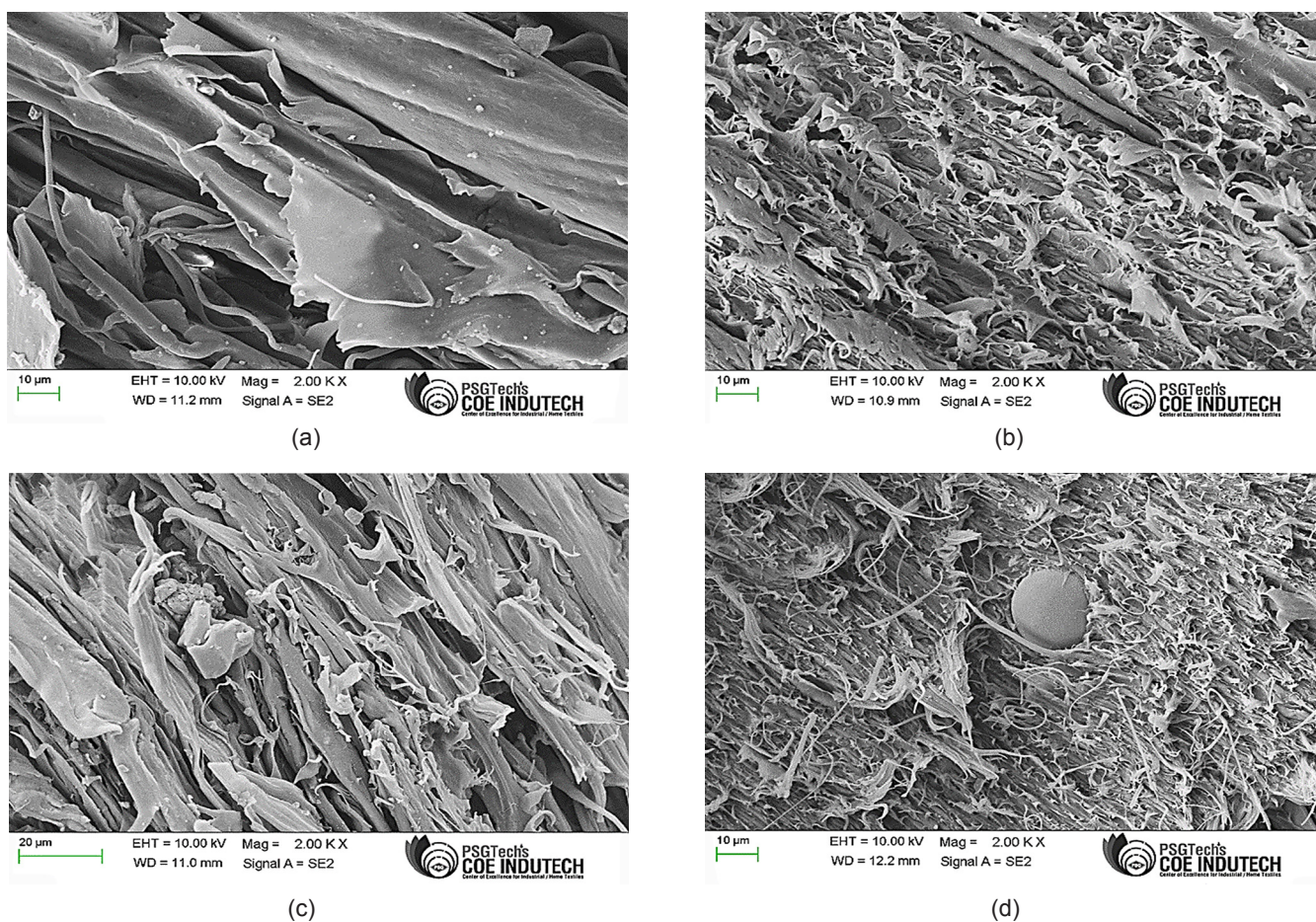


Figure 10. SEM images of tensile fractured (a) 50PP50PA (b) 50PP50PA5C (c) 50PP50PA3HGM (d) 50PP50PA5C3HGM.

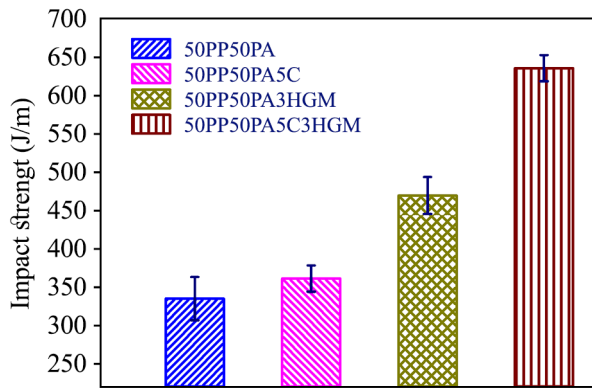
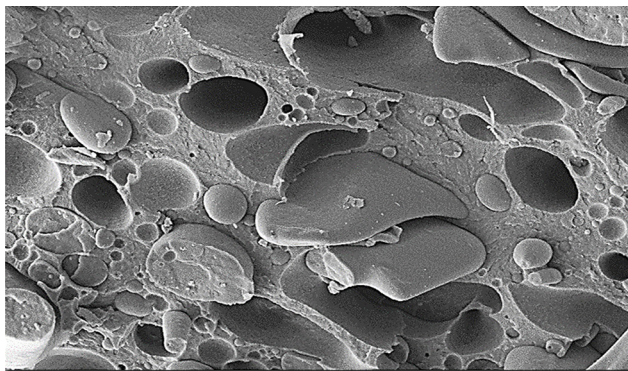


Figure 11. Impact Strength of 50/50 PP/PA6 blends and their composites in the presence and absence of PP-g-MA and HGMs.

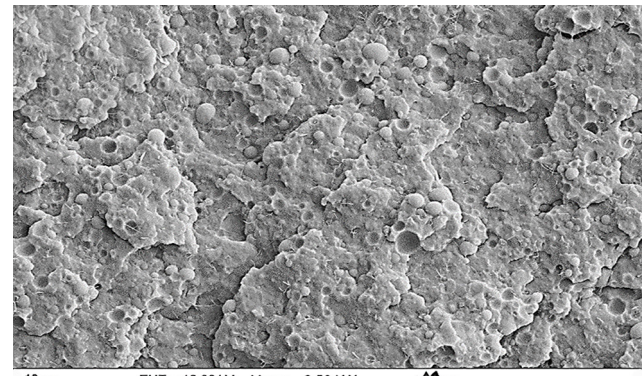
the viscosity (Figure 4) decreases, and the increase in crystallinity of PP and PA6 phases is responsible for the increase in tensile properties. While the incorporation of HGMs and PP-g-MA to a 50PP50PA6 blend results in a slight decrease in viscosity (Figure 4), an increase in crystallinity of PP and PA6 phases, a significant refinement in morphology, and the formation of

finer fibrils (Figure 10) are the major reasons for the highest increase in tensile properties. The finer fibril formation results in a greater number of fibrils resisting tensile deformation, and interfacial compatibilization provides additional deformation resistance for the 50PP50PA6 blend containing HGMs and PP-g-MA.

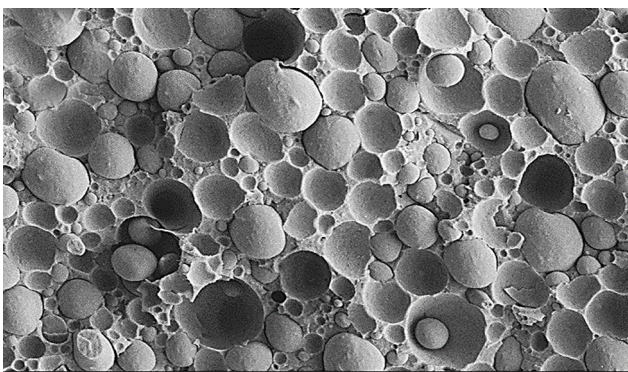
The impact properties of 50PP50PA6 blends and their composites are depicted in Figure 11. It demonstrates that the impact strength of 50PP50PA6 is 334 J/m. The 50PP50PA6 blend containing PP-g-MA improves impact strength to 470 J/m, representing a 40.7% improvement as compared to the neat blend. While the addition of HGMs to the 50PP50PA6 blend increases impact strength marginally. But, the incorporation of the compatibilizers PP-g-MA and HGMs in the 50PP50PA6 blend reveals the greatest increase in impact strength to 635 J/m, a 90.1% improvement as compared to the neat blend. To understand the fracture mechanism, SEM studies were carried out over the fractured surface of the 50PP50PA6 blend and its composites. Figure 12 depicts impact fractured SEM images of the 50PP50PA6 blend



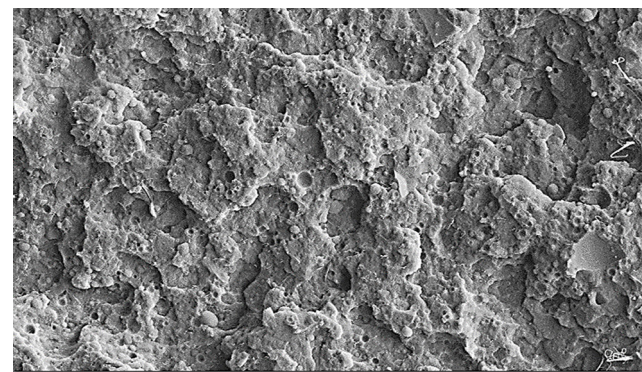
(a)



(b)



(c)



(d)

Figure 12. SEM images of impact fractured (a) 50PP50PA (b) 50PP50PA5C (c) 50PP50PA3HGM (d) 50PP50PA5C3HGM.

Table 5. Comparison of the impact properties obtained from the literature and this study.

No	PP/PA6 Blend Composition	Compatibilizer	Fillers	% Impact Strength Enhancement	References
1	80/20	PP-g-MA	Nanosilica (0.9 wt.%)	42.45	32
2	20/80	PP-g-MA	Wollastonite (30 wt.%)	65.64	33
3	30/70	SEBS-g-MA	Organoclay (4 wt.%)	11.3	34
4	50/50	Ethylene-Octene Copolymer	Organoclay (4 wt.%)	-8.9	35
5	50/50	PP-g-MA	HGMs (3 wt.%)	90.1	This work

Note: Negative sign indicates the decrease in impact strength.

and its composites. The SEM image of the 50PP50PA6 blend is shown in Figure 12a. It demonstrates that phase dislodgement is due to insufficient interfacial adhesion between the PP and PA6 phases. While the compatibility of 50PP50PA6 blend with PP-g-MA reveals droplet retention during impact fracture due to reactive compatibilization (Figure 12b). This is why the impact properties of the 50PP50PA6 blend containing PP-g-MA have enhanced significantly. While the incorporation of 3 wt.% HGMs in 50PP50PA6 blend results in fibril pull out and formation of holes, and fibril breakup is responsible for the marginal improvement in impact properties. The SEM image of the 50PP50PA6 blend containing HGMs and PP-g-MA is represented in Figure 12d. Because of the refined morphology and reactive compatibilization, the majority of the droplets are not dislodged. Furthermore, the refined morphology can absorb more energy, which is why the impact property enhancement is greatest for the 50PP50PA6 blend containing PP-g-MA and HGMs. In light of the significant increase in the 50PP50PA6 blend containing HGMs and PP-g-MA, the literature on PP/PA6 blends based composites was compared with the findings of this study and the findings are tabulated in Table 5 [32-35]. It shows that PP-g-MA, SEBS-g-MA, and ethylene-octene copolymers were utilized as a compatibilizer in PP/ABS blend [32-35]. When a low concentration of nanosilica is added to a PP/ABS blend with PP-g-MA, the impact strength increases by 42.45% when is compared to the neat blend [32]. Impact properties reduced when PP:PA6 was mixed in 50:50 with organoclay and ethylene-octene copolymer [35]. In this study, a 50:50 ratio of PP:PA6 containing HGMs and PP-g-MA improved impact strength by 90.1%. The increase in impact properties is the highest so far achieved for PP/PA6 blend and its composites.

CONCLUSION

The incorporation of HGMs-filled 50PP50PA6 blends and their composites using melt-mixing was investigated. HGMs used in this work were characterized using SEM and appear to be rough. The interaction of HGMs with the PA6 phase was revealed by FTIR spectroscopy. FTIR spectroscopy was also used to characterize the melt-interfacial reaction between the PP-g-MA and PA6 phases. Because of chemical bonding at the interface of the blend, the viscosity of the maleated 50PP50PA6 blend is higher. Furthermore, the addition of HGMs to the 50PP50PA6 blends and their composites reduces viscosity, indicating improved processability. The 50PP50PA6 blend exhibited co-continuous morphology with droplets. The incorporation of PP-g-MA in the 50PP50PA6 blend resulted in refined co-continuous morphology containing droplets. Furthermore, the presence of HGMs in the 50PP50PA6 blend results in elongated fibrillary morphology. In addition, the presence of HGMs and PP-g-MA in the 50PP50PA6 blend demonstrated refined morphology. WAXRD analysis of a 50PP50PA6 blend and its composites revealed the formation of α -form PP and PA6 crystals. The HGMs-filled 50PP50PA6 blend containing PP-g-MA showed the best mechanical properties. It was caused by an enhanced crystallinity of the PP and PA6, refined morphology formation, and interaction between the HGMs and the PA6 phase. The addition of PP-g-MA and HGMs to the 50PP50PA6 blend revealed fine fibrils on the tensile fracture surface, which was another reason for the improved tensile properties. The impact fracture SEM image of the 50PP50PA6 blend containing PP-g-MA and HGMs revealed that the droplets of PA6 were intact over the

surface, indicating resistance to the impact failure. DMA studies revealed the stiffening effect of HGMs in a 50PP50PA6 blend with and without PP-g-MA.

CONFLICTS OF INTEREST

The authors declare that they have no conflicts of interest.

REFERENCES

1. Qingzhang Z, Zhilong H, Hao Z, Zhenqing W, Da X (2021) Experimental study on resisted water pressure for connecting welds of polypropylene plastic plates in underground silos. *Plast Rubber Compos* 51: 316-324
2. Li JW, Yang K, Song L, Han L, Feng YK (2015) Non-isothermal crystallisation of polypropylene/hollow glass microspheres composites. *Plast Rubber Compos* 44: 68-73
3. Peng XH, Li MX, Zou HW, Fan P, Liu PB (2012) Morphology and properties of functionalised MWNT/Polypropylene Composites. *Plast Rubber Compos* 41: 23-28
4. Asumani O, Paskaramoorthy R (2020) Fatigue and impact strengths of kenaf fibre reinforced polypropylene composites: Effects of fibre treatments. *Adv Compos Mater* 30:103-115
5. Bonda S, Mohanty S, Nayak SK (2014) Influence of compatibilizer on mechanical, morphological and rheological properties of PP/ABS blends. *Iran Polym J* 23: 415-425
6. Wang K, Li T, Xie S, Wu X, Huang W, Tian Q, Tu C, Yan W (2019) Influence of organo-sepiolite on the morphological, mechanical, and rheological properties of PP/ABS blends. *Polymers* 11: 1493
7. Lee HG, Sung Y-T, Lee YK, Kim WN, Yoon HG, Lee HS (2009) Effects of PP-G-Mah on the mechanical, morphological and rheological properties of polypropylene and poly(acrylonitrile-butadiene-styrene) blends. *Macromol Res* 17: 417-423
8. Shi D, Ke Z, Yang J, Gao Y, Wu J, Yin J (2002) Rheology and morphology of reactively compatibilized PP/PA6 blends. *Macromolecules* 35: 8005-8012
9. Shi D, Hu G-H, Ke Z, Li RKY, Yin J (2006) Relaxation behavior of polymer blends with complex morphologies: Palierne emulsion model for uncompatibilized and compatibilized PP/PA6 blends. *Polymer* 47: 4659-4666
10. Tseng F-P, Lin J-J, Tseng C-R, Chang F-C (2001) Poly(oxypropylene)-amide grafted polypropylene as novel compatibilizer for PP and PA6 blends. *Polymer* 42: 713-725
11. Palacios JK, Sangroniz A, Eguiazabal JI, Etxeberria A, Müller AJ (2016) Tailoring the properties of PP/PA6 nanostructured blends by the addition of nanosilica and Compatibilizer Agents. *Eur Polym J* 85: 532-552
12. Pinheiro LA, Bittencourt CS, Canevarolo SV (2009) Real time assessment of the compatibilization of polypropylene/polyamide 6 blends during extrusion. *Polym Eng Sci* 50: 826-834
13. Kumar N, Mireja S, Khandelwal V, Arun B, Manik G (2017) Light-weight high-strength hollow glass microspheres and bamboo fiber based hybrid polypropylene composite: A strength analysis and morphological study. *Compos B Eng* 109: 277-285
14. Charière R, Marano A, Gélébart L (2020) Use of composite voxels in FFT based elastic simulations of hollow glass microspheres/polypropylene composites. *Int J Solids Struct* 182-183: 1-14
15. Gogoi R, Manik G, Arun B (2019) High specific strength hybrid polypropylene composites using carbon fibre and hollow glass microspheres: Development, characterization and comparison with empirical models. *Compos B Eng* 173: 106875
16. Gogoi R, Kumar N, Mireja S, Ravindranath SS, Manik G, Sinha S (2018) Effect of hollow glass microspheres on the morphology, rheology and crystallinity of short bamboo fiber-reinforced hybrid polypropylene composite. *JOM* 71: 548-558
17. Gogoi R, Manik G (2021) Development of thermally conductive and high-specific strength polypropylene composites for thermal

- management applications in automotive. *Polym Compos* 42: 1945-1960
18. Kang B-H, Yang X-Y, Lu X (2019) Effect of hollow glass microsphere on the flame retardancy and combustion behavior of intumescent flame retardant polypropylene composites. *Polym Bull* 77: 4307-4324
 19. Yağci Ö, Eker Gümüş B, Taşdemir M (2020) Thermal, structural and dynamical mechanical properties of hollow glass sphere-reinforced polypropylene composites. *Polym Bull* 78: 3089-3101
 20. Bose S, Bhattacharyya AR, Häußler L, Pötschke P (2009) Influence of multiwall carbon nanotubes on the mechanical properties and unusual crystallization behavior in melt-mixed co-continuous blends of Polyamide6 and acrylonitrile butadiene styrene. *Polym Eng Sci* 49: 1533-1543
 21. Panda B, Bhattacharyya AR, Kulkarni AR (2011) Ternary polymer blends of polyamide 6, polypropylene, and acrylonitrile-butadiene-styrene: Influence of multiwalled carbon nanotubes on phase morphology, electrical conductivity, and crystallization. *Polym Eng Sci* 51: 1550-1563
 22. Ishida H, Scherbakoff N (1991) Interphase compatibilization of composites with immiscible blends as matrix: Glass beads filled nylon 6/polypropylene blend-composite. *Makromol Chem, Macromol Symp* 50:157-170
 23. Mutua FN, Lin P, Koech JK, Wang Y (2012) Surface modification of hollow glass microspheres. *Mater Sci Appl* 3: 856-860
 24. Huang C, Huang Z, Lv X, Zhang G, Wang Q, Wang B (2016) Surface modification of hollow glass microsphere with different coupling agents for potential applications in phenolic syntactic foams. *J Appl Polym Sci* 134: 44415-44423
 25. Wu S (1982) *Polymer interface and adhesion*. New York: Dekker
 26. Lohar G, Tambe P, Jogi B (2020) Influence of dual compatibilizer and carbon black on mechanical and thermal properties of PP/ABS blends and their composites. *Compos Interfaces* 27: 1101-1136
 27. Xu G, Qin S, Yu J, Huang Y, Zhang M, Ruan W (2015) Effect of migration of layered nanoparticles during melt blending on the phase morphology of poly (ethylene terephthalate)/polyamide 6/montmorillonite ternary nanocomposites. *RSC Adv* 5: 29924-29930
 28. Mader-Arndt K, Kutelova Z, Fuchs R, Meyer J, Staedler T, Hintz W, Tomas J (2014) Single particle contact versus particle packing behavior: Model based analysis of chemically modified glass particles. *Granul Matter* 16: 359-375
 29. Zhou X, Zhang P, Jiang X, Rao G (2009) Influence of maleic anhydride grafted polypropylene on the miscibility of polypropylene/polyamide-6 blends using ATR-FTIR mapping. *Vib Spectrosc* 49: 17-21
 30. Wang Q, Liu C, Chen Z (2001) Pan-milling preparation of polypropylene-graft-maleic anhydride and its compatibilizing effect on polyamide 6/polypropylene blend. *Polymer J* 339: 522-527
 31. Wang Y, Sun W, Liu S, Ji H, Chen X, Zhu H, Zhao H, Ma Y, Xie L (2020) The formation of a highly oriented structure and improvement of properties in PP/PA6 polymer blends during extrusion-stretching. *Polymers* 12: 878-892
 32. Palacios JK, Sangroniz A, Eguiazabal JI, Etxeberria A, Müller AJ (2016) Tailoring the properties of PP/PA6 nanostructured blends by the addition of nanosilica and compatibilizer agents. *Eur Polym J* 85: 532-552
 33. Wang Q, Liu C, Chen Y (2001) Studies on PA6-PP-wollastonite composite compatibilised by PP-graft-maleic anhydride prepared via pan milling. *Plast Rubber Compos* 30: 363-369
 34. Ishak ZM, Chow WS, Takeichi T (2008) Influence of SEBS-G-MA on morphology, mechanical, and thermal properties of PA6/PP/Organoclay nanocomposites. *European Polym J* 44: 1023-1039
 35. Wahit MU, Hassan A, Rahmat AR, Lim JW, Ishak ZA (2006) Effect of organoclay and ethylene-octene copolymer inclusion on the morphology and mechanical properties of polyamide/polypropylene blends. *J Reinf Plast Compos* 25: 933-955